Particle
& Particle Systems Characterization
www.particle-journal.com
www.MaterialsViews.com

Single-Cell Investigations of Silver Nanoparticle–Bacteria Interactions

*Sudarsan Vishnupriya, Kamalesh Chaudhari, Ramya Jagannathan, and Thalappil Pradeep**

Interaction of bacteria with citrate-reduced silver nanoparticles (AgNPs) of size 25 nm ± 8.5 nm is studied using Raman spectroscopy in conjunction with plasmon resonance imaging of single bacterial cells. Distribution of isolated nanoparticles (NPs) inside *Escherichia coli* (ATCC 25922; *E. coli*) is observed by hyperspectral imaging (HSI) as a function of incubation time. Time-dependent degradation of bacterial DNA upon incubation of AgNPs with *E. coli* is proven by Raman spectroscopic studies. While attachment of NPs is evident in HSI, molecular changes are evident from the surface-enhanced Raman spectra of adsorbed DNA and its fragments. Distinct enhancement of DNA features is observed upon interaction of AgNPs and the number of such distinct features increases with incubation time, reaches a maximum, and decreases afterwards. This systematic interaction of DNA with the NPs system and its gradual chemical evolution is proven by investigating isolated plasmid DNA. A comparative Raman study with silver ions has shown that DNA features are observable only when bacteria are incubated with AgNPs. Energetics of interaction examined with microcalorimetry suggests the exothermicity of -1.547×10^{10} cal mol^{-1} for the NP–bacteria system. Specific interaction of AgNPs with exocyclic nitrogen present in the bases, adenine, guanine, and cytosine, leads to the changes in DNA.

1. Introduction

One of the rapidly evolving areas of the applications of noble metal nanoparticles (NPs) is water purification.[1,2] Various nanomaterial-based strategies have been developed for the remediation of diverse environmental contaminants, including microbes, in the recent past.[3–5] Silver nanoparticles (AgNPs)-based disinfection is one of the simplest remediation strategies for microbial contamination and has been used from ancient times.[6,7] Recent advancement in the understanding of the chemistry of noble metal NPs has contributed to their intense use in antibacterial applications and this is one of the major reasons for AgNPs to be the most economically significant nanomaterial in use today. Utility of such materials has been demonstrated in recent past with the development of an affordable water purifier using AgNP–biopolymer composites.[8] It is important to point out that noble metal NPs are important in oxidation, dehalogenation, and CH-bond activation and several of these properties have been used in environmental applications.[1,9–11] In the context of microbial disinfection, the mechanism behind the action of AgNPs is still an issue of debate. We shall briefly discuss below the status of the current understanding of the area.

Major events upon exposure of AgNPs to microorganisms are reported to be: i) generation of free radicals reactive oxygen species (ROS),[12,13] ii) subsequent incorporation of AgNPs in the membrane, as well as free radical induced structural changes in it,[14,15] iii) increase in cell permeability to Ag^+ ions and AgNPs[14,16] due to (ii), iv) loss of DNA replicability and protein activity, resulting in the inhibition of cell growth,[17,18] v) accumulation of protein precursors, destabilization of the outer membrane, collapse of the plasma membrane potential and depletion of intracellular adenosine triphosphate (ATP) levels, especially at short exposures,[19] and vi) inhibition of respiratory chain dehydrogenases.[15] There are also conflicting reports on all of these with some studies favoring specific pathways.[13,17,20] Model studies have been performed to understand the interaction of NPs with cellular ingredients such as proteins,[21] lipids,[22] and DNA bases.[23] Recently, Alvarez and co-workers[24] observed that silver ions leaching from AgNPs are the major reason for the antibacterial property of AgNPs. Despite all of these, our knowledge about the microscopic details of disinfection is still inadequate. Absence of the closer view of the interaction of AgNPs at single-cell level prompted us to investigate it at this scale, aided by techniques such as confocal Raman microscopy (CRM) along with the scattering-based hyperspectral imaging (HSI), which enable visual,

S. Vishnupriya, Prof. T. Pradeep
DST Unit on Nanoscience (DST UNS) and
Thematic Unit of Excellence
Department of Chemistry
Indian Institute of Technology Madras
Chennai 600036, India
E-mail: pradeep@iitm.ac.in
K. Chaudhari
DST Unit on Nanoscience (DST UNS)
Department of Chemistry
Department of Biotechnology
Indian Institute of Technology Madras
Chennai, 600036, India
Dr. R. Jagannathan
Chemical Lab
CSIR-Central Leather Research Institute
Chennai 600020, India

DOI: 10.1002/ppsc.201300165

spectral, and chemical observation. Apart from imaging, we have performed isothermal calorimetric studies to understand the thermodynamic aspects of a single AgNP–bacterium interaction with the model organism, *Escherichia coli (E. coli)*.

2. Results and Discussion

2.1. Hyperspectral Analysis

As citrate-reduced AgNPs are well known, their properties are not discussed in detail. Transmission electron microscopy (TEM) images of AgNPs show the particles to be in the range of 25 ± 8.5 nm (Figure S1, Supporting Information) and its polydisperse nature is clearly observed in the HSI image (Figure S2, Supporting Information) where distinctly different particles are seen. The phenomenon of accumulation of AgNPs on bacteria was proved by HSI (**Figure 1**). AgNPs are efficient scatterers and provide good contrast as compared with the cellular components, which enable us to image even a single AgNP and localize it inside or on the periphery of a bacterium. But low resolution and poor scattering limit the HSI of bacteria for in situ observations of the interaction of NPs with cellular components or biomolecules. Figure 1A shows large-area image of *E. coli* treated with AgNPs. Scattering spectra collected from different spots are also shown in Figure 1B and the inset shows the magnified HSI image of a single bacterium, treated with AgNPs. Hyperspectral image of the control bacteria (untreated) is shown in Figure S3 (Supporting Information). AgNPs show a sharp localized surface plasmon resonance peak with large scattering intensity while spectrum of the bare cell membrane of the bacteria shows a broad scattering spectrum with maximum in the blue–green region (400–550 nm). The scattering intensity from the bacterial cell membrane is an order of magnitude weaker than from the NPs. Images of AgNPs-treated bacteria clearly show that AgNPs attach on them (see the circled regions in Figure 1). Time-dependent HSI observations of AgNPs-treated bacteria were made to see the uptake of NPs by bacteria. We see that the number of AgNPs attached to the bacterium has increased with incubation time. Lysis of the bacteria was observed when the treatment time of AgNPs increased for more than an hour (Figure S4, Supporting Information).

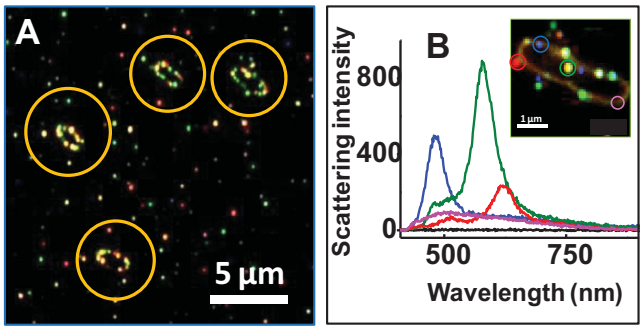

Figure 1. A) Hyperspectral image of *E. coli* after treatment with AgNPs. B) The inset shows an enlarged image of a single bacterium treated with NPs and scattering spectra corresponding to the encircled particles on the bacterium. Colors of the traces correspond to the circles in which a specific particle is selected. The black trace corresponds to the background. The bacterial cell membrane shows a weak scattering spectrum and the scattering spectrum of the NPs shows distinct peak maxima.

2.2. Raman Spectroscopic Analysis

2.2.1. SERS of AgNPs

It may be noted that previous Raman spectroscopic studies of AgNPs and bacteria were principally to detect isolated bacterium[25] and to distinguish different species of bacteria,[26,27] utilizing the surface-enhanced Raman scattering (SERS). The present work we believe is the first report using Raman spectroscopy to know the in situ interaction of AgNPs with single bacteria. Internalization of AgNPs was observed by Raman spectroscopy. Due to the SERS property of AgNPs, the penetration of AgNPs inside the bacterium was reflected as 10- to 100-fold intensity enhancement of the Raman signals of the molecules within a bacterium (**Figure 2**), when spectra are compared without and with AgNPs (Figure 2A,C). This is evident in the Raman images of single bacterial cells also (Figure 2B,D). The accumulation of AgNPs on bacteria is initiated due to good affinity of silver for sulfur-[28] and amine-[29]containing molecules such as proteins present on the outer membrane. It is also supported by isothermal calorimetry (ITC) studies, discussed later.

2.2.2. Time-Dependent Raman Measurements of Bacteria Treated with AgNPs

Temporal Raman spectroscopic observations were performed on the bacteria incubated with AgNPs for 5, 10, 20, 30, and 60 min (Figure S5, Supporting Information). As spectra from single bacterium change significantly from cell to cell, multiple bacteria at each time of incubation were examined. However,

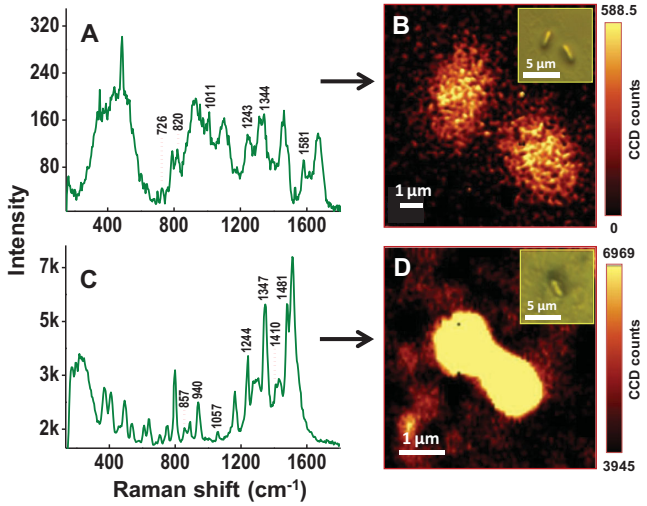

Figure 2. Raman spectra and Raman images of a single bacterium without (A,B) and with treatment (C,D) of AgNPs for 10 min. Intensity scales clearly indicate the large enhancement in the Raman scattering intensity of AgNPs-treated *E. coli* as compared with untreated *E. coli*.

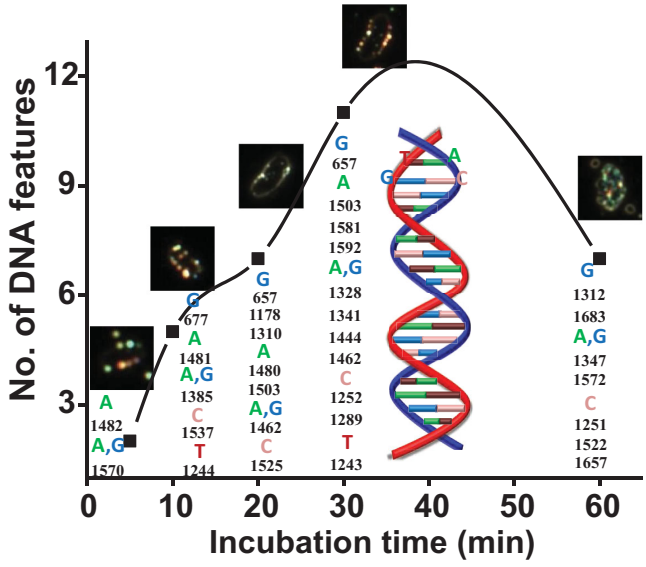

Figure 3. Comparison of the observed number of DNA peaks arising from bacteria treated with AgNPs for various incubation times (5, 10, 20, 30, and 60 min). Corresponding dark-field optical images of a typical bacterium are shown. This comparison clearly shows increase in the number of DNA peaks with the increase in incubation time following a decrease of DNA peaks when the incubation time 1 h. The assignments are based on various reports.[30–38]

spectra were reproducible for both treated and untreated bacteria, in terms of the occurrence of the same spectral features, but not the peak shape. This kind of variation is seen in SERS of molecular mixtures as in this case.[25–27] The occurrence of the same features suggests that with time, molecular-specific interaction of AgNPs with the inner structures of the bacteria occurred as compared with the outer structure. To verify the reproducibility of this data, spectra from five separate bacteria were measured and compared (Figure S5, Supporting Information). Time-dependent data have shown Raman features corresponding to proteins, lipids, carbohydrates, RNA, and DNA. Enhanced intensities of these features indicate the presence of AgNPs on the outer membrane as well as inside the bacteria. Peaks in the Raman spectra of AgNPs-treated and untreated bacteria were assigned using previous reports of Raman spectroscopy of bacteria (Table S6, Supporting Information).[30–38] It is known that AgNPs enhance the membrane permeability, which leads to the entry of particles inside the bacteria[13] and supposedly affect the growth of bacteria by interacting with the DNA.[17] From the experimental data, we observed that the number of distinct Raman peaks arising from the DNA of *E. coli* increases with incubation time of AgNPs; however, after 60 min, this number is reduced (**Figure 3**). It is important to recall that the interaction of AgNPs with mammalian cells leads to DNA degradation.[39,40] The degradation of DNA may be due to the disruption of the electron transfer pathway in mitochondrial respiratory chain by AgNPs, which leads to the production of ROS and interruption of ATP synthesis.[40] Therefore, it is reasonable to conclude that the DNA features we observed in Figure 3 are due to their degradation products. From the Raman study, it is observed that the Raman scattering intensity of the nucleotide bases of DNA such as adenine (A), guanine (G), and cytosine (C) peaks were enhanced, whereas thymine (T) showed only limited enhancement. It has been shown that there can be strong interaction between amines and AgNPs.[29] The interaction of AgNPs with A, G, and C is strong, possibly due to the interaction of AgNPs with the exocyclic nitrogen present in these bases, and this is responsible for the enhancement in the peak intensities of the Raman spectra of these bases. On the other hand, T, devoid of this exocyclic amine group, interacts weakly with AgNPs.[23] Independent studies were done to calculate the SERS enhancement factors for bases treated with AgNPs as explained by Pavan Kumar et al.[41] The enhancement factors determined were in the order, C (9×10^4) > G (7×10^4) > A (5×10^4) > T (2×10^4). From these observations, we concluded that apart from the major effect of AgNPs on membrane damage,[15] they are highly specific towards bacterial DNA. We also observed the lysis of bacteria treated with AgNPs for a period more than an hour. It is supported by the time-dependent HSI images and bright field optical images of the bacteria treated with AgNPs (Figures S4 and S7, Supporting Information). The damage of bacterial membrane was observed in the bacteria treated with AgNPs for more than an hour. However, when the incubation time was less than an hour, observable morphological changes were not seen.

2.2.3. Comparison of Plasmid DNA and E. coli Cells, Both Treated with AgNPs

To confirm that specific peaks in the Raman spectra of *E. coli* cells treated with AgNPs are indeed from DNA, plasmid DNA was isolated from the *E. coli* cells and it was incubated with AgNPs for 20 min and Raman measurements were carried out. The DNA peaks from the treated (20 min) *E. coli* cells were found to be similar to the peaks of plasmid DNA treated with AgNPs (**Figure 4**). The interaction of plasmid DNA with AgNPs also exhibits an enhancement in the peak intensity of the bases

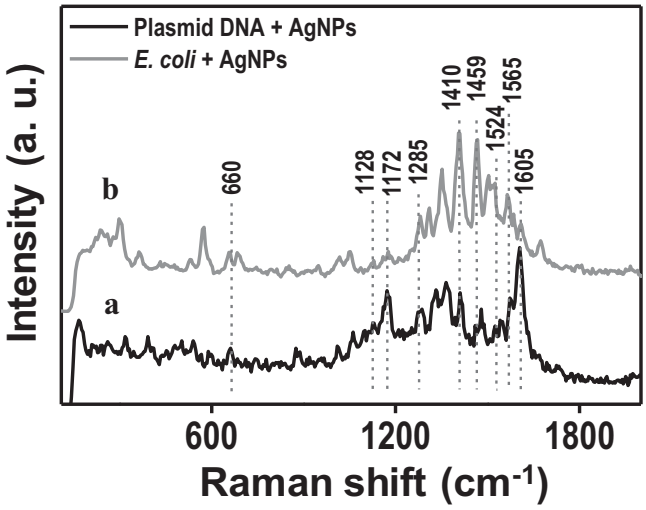

Figure 4. Comparison of the Raman spectra of *E. coli* plasmid DNA and whole *E. coli* cell, both treated with AgNPs. a) Raman spectrum of plasmid DNA treated with AgNPs for 20 min and b) Raman spectrum of *E. coli* cell treated with AgNPs for 20 min. Similar peaks seen are noted.

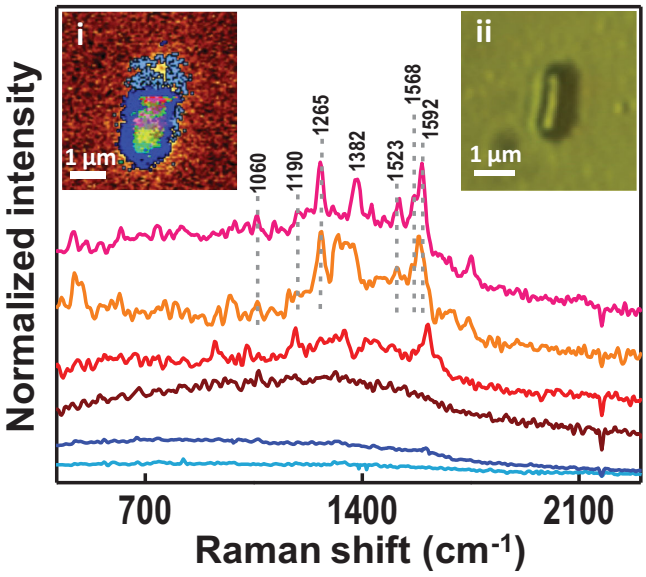

Figure 5. Raman image spectra obtained by the cluster analysis of the Raman image of a single bacterium. Inset i) shows the cluster analysis of the Raman image, which is merged with the original Raman image of a bacterium and inset ii) shows the corresponding optical image of the bacterium imaged. Each specific region in the bacterium has its corresponding Raman spectrum and it is represented in different colors. These spectra are observed from different regions of a single bacterium. There are additional component spectra, which are weaker and are not shown.

such as A, G, and C. The peak intensity of T was weak even in this case also. This observation confirms that there is a strong and specific interaction between AgNPs and A, G, and C bases, while T is weak in its interaction. The assignments of Raman peaks of *E. coli* plasmid DNA treated with AgNPs are shown in Table S8 (Supporting Information).[31,35,37,42–44]

2.3. Cluster Analysis

It was important to see if specific peaks are localized in distinct regions of the bacterium. For this, cluster analysis of the Raman spectra was carried out. Using cluster analysis, thousands of spectra in the Raman spectral image can be classified according to similarities of their features and the image can be mapped to spatially localize the point of interest.[45] **Figure 5** shows the cluster analysis of the Raman image of nanoparticle-treated *E. coli* cell. Different Raman spectra are represented in different colors after the analysis. The peaks corresponding to DNA (1592, 1568, 1523, 1382), proteins (1265,[31] 1190), and lipids (1060) are shown in Figure 5 and these peak assignments are represented in Table S6 (Supporting Information). All the features of each of the components of the cell are not seen, possibly due to the reduced aquisition time used for image collection. The central portions of the image marked with different colors are due to regions with specific Raman spectra, rich in DNA and protein features. Since Raman spectra obtained from cluster analysis are averages of spectra in that particular region, they contain multiple features. But spectra shown in Figure 4 are single-spot spectra obtained by manual monitoring; hence, they show features only from the location where AgNP–DNA interaction happens. This result supports the entry of AgNPs into the bacteria and their interaction with silver-binding proteins and DNA.[28] Most of the intensity in the outer region corresponds to the background and unresolved structures. Upon comparison with the optical image, it is clear that the DNA and protein features are localized within the bacterial contour. The plasmid DNA features (1524, 1565 cm^{-1}) of Figure 4 are clearly manifested in the spectra after cluster analysis.

2.4. Raman Measurements of Bacteria Treated with Ag^+ Ions

Previous studies have proposed that leaching of silver ions from AgNPs affected the DNA of a bacterium leading to its death.[16] To further probe the role of Ag^+ ions, bacteria were incubated with Ag^+ ions at 0.6×10^{-6} M for various time intervals (5, 10, 20, 30, and 60 min) and Raman spectroscopic measurements were done as in the case of AgNPs (Figure S9, Supporting Information). No enhancement in the peaks of Raman spectra was observed at any time interval, unlike in the case of *E. coli* treated with AgNPs. Compared with untreated *E. coli*, which gives 120 counts in the Raman spectrum for a major peak (Figure 2), the Raman spectra of *E. coli* treated with Ag^+ were weaker (Figure S9, Supporting Information). Consequently, several features were poorly reproducible. From the assignment of certain reproducible features, it is observed that DNA features are not enhanced unlike in the case of AgNPs but Raman features for proteins, carbohydrates, and lipids were observed (Table S10, Supporting Information). Ag^+ ions have good antibacterial property and several mechanisms have been proposed in this context.[46–48] Hyperspectral analysis of *E. coli* treated with Ag^+ ions has shown lysis of the cell membrane. Lysis begins after 30 min and can be seen clearly after 1 h of incubation (Figure S11, Supporting Information). AgNPs may leach silver ions within the bacteria and they may be responsible for part of the bactericidal action. The interaction of NPs with specific bacterial components like DNA, proteins, carbohydrates, and lipids was observable only in the case of AgNPs, while the interaction of Ag^+ ions with bacteria was not observable with Raman spectroscopy at the single-cell level as there is no enhancement in the Raman features.

2.5. Isothermal Calorimetry Study

We performed ITC studies to understand the strength of interaction between AgNPs and *E. coli*. ITC responses recorded during the titration of AgNPs against *E. coli* (**Figure 6**A) and the integrated calorimetric response plotted against the molar ratio of *E. coli*/AgNPs (Figure 6B) suggests strong interaction between the two. The exothermic and sigmoidal response for the binding with *E. coli* substrates suggests that as the titration progresses, AgNPs try to occupy all the possible sites of *E. coli* present in the ITC cell and after a few injections, no more AgNPs are left in the cell to occupy the sites, which leads to saturation. We have fitted the integrated calorimetric response with a model of single set of N identical sites on a substrate. However, multiple interactions do take place when bacteria are

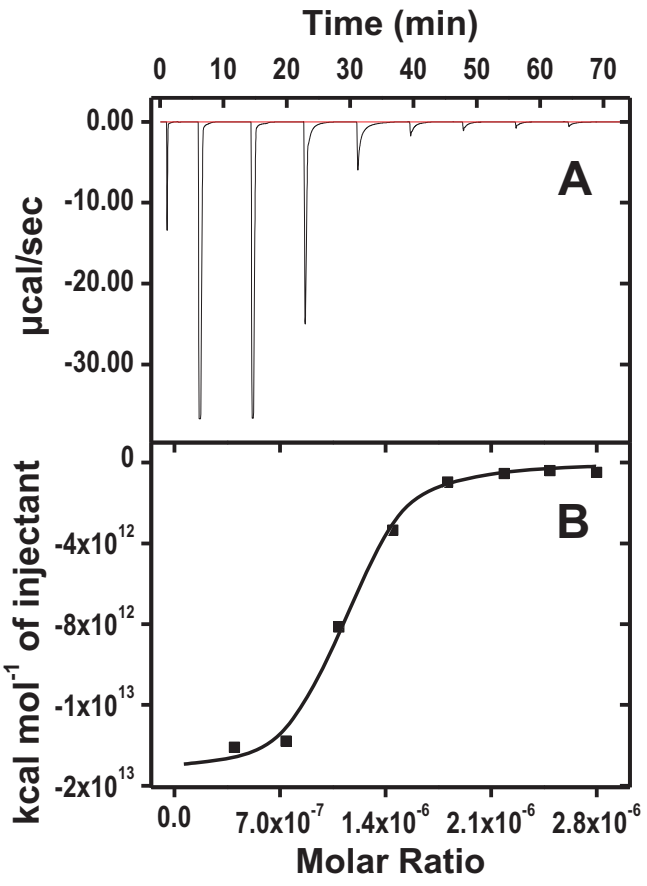

Figure 6. A) ITC responses for the titration of *E. coli* with the AgNPs. B) Integrated calorimetric response plotted against the molar ratio of *E. coli*/AgNPs (concentrations: 1.62×10^{-14} M/1.2×10^{-9} M). Concentration calculations are explained in the Experimental Section.

injected into a pool of AgNPs. The major interaction is believed to be the attachment of AgNPs on bacterial surface and as time progresses, there is possible diffusion of AgNPs through the cell wall of the bacteria and subsequent intracellular interactions with proteins and DNA, as observed in Raman spectroscopy. Also citrate-stabilized AgNPs tend to aggregate with time, especially when they are in reactive environment, like in contact with the bacteria. Part of the interparticle interaction energy released during aggregation is also added to the measured exothermicity. As compared with other macromolecules commonly studied using the ITC technique, *E. coli* substrates have large number of binding sites for AgNPs due to the presence of multiple functionalities and very large surface area (compared to NPs). Hence, this system is far more complex than typical ITC studies for a single ligand–substrate pair. Although the data can be fitted with a model of single set of N identical sites on a substrate, we could not extract the realistic number of binding sites or binding energy per particle due to the additional processes outlined above. Collectively, all the above interactions give an initial exothermicity of -1.547×10^{10} cal mol^{-1} of bacteria, which proves the high strength of interaction. This value of exothermicity is very high as compared with those that are observed for simpler interactions between biomolecules[49,50] but while considering the complexity of the system involving multiple interactions taking place at the same time, these values can be rationalized. Reproducibility of this data was ascertained (Figure S12, Supporting Information).

3. Conclusions

Raman and HSI were performed to understand the interaction of AgNPs with single bacterial cells. HSI supports the accumulation of AgNPs on the bacteria. Raman spectra and corresponding Raman images confirm the distribution of AgNPs within the bacteria. The time-dependent Raman study shows that when the incubation time exceeds an hour, degradation of DNA occurs, causing decrease in specific Raman signals of nucleotides. The interaction of AgNPs occurs mainly with proteins and DNA and their distribution inside the bacteria was shown by the cluster analysis of the Raman image of AgNPs-treated bacterium. While the interaction of AgNPs with bacteria was observable at the single-cell level due to SERS, Ag^+ ion interaction was not observable. Initial exothermicity of -1.547×10^{10} cal mol^{-1} was observed in ITC experiment, which proves the high strength of AgNP–*E. coli* interaction. While the present results confirm chemical degradation of DNA at NPs, additional systematic studies with fluorescence-activated cell sorting (FACS), inductively coupled plasma mass spectrometry (ICP-MS), and scanning transmission electron microscopy (STEM) are necessary to understand the fate of the living system. The accumulation of the Raman spectra from the particle from which plasmon spectrum is collected simultaneously will enable tracking of chemical processes at NPs in real time. This would provide dynamics of such events and we are in the process of developing such measurements.

4. Experimental Section

Materials: Silver nitrate and trisodium citrate were purchased from Rankem and Qualigens. All chemicals were used without further purification.

Synthesis of AgNPs: AgNPs were synthesized by the Turkevich method.[51] In this method, about 17 mg of silver nitrate was mixed with 100 mL of deionized water (1×10^{-3} M) and kept for heating at 100 °C. To this, 40 mg of trisodium citrate was added and boiled for 10 min, until a pale yellow color indicating the reduction of Ag^+ ions was obtained. The solution was cooled immediately under tap water. The final suspension of AgNPs shows a plasmon absorption peak at 420 nm. These particles are in the size range of 25 ± 8.5 nm as confirmed by TEM.

Incubation of E. coli Cells and Plasmid DNA with AgNPs and Ag^+ Ions: An overnight culture of *E. coli* (ATCC 25922) cells was subcultured in LB broth and grown at 37 °C with shaking for 4 h to obtain a log phase culture. The bacterial count was monitored by the conventional plate count method and by reading the optical density at 600 nm. Bacterial culture was centrifuged at 3000 rpm for 5 min and the resultant pellet was washed twice with triply distilled water and subsequently dispersed to eliminate broth interference in the experiment. About 5×10^5 cells from this were taken and added to 1×10^{-3} M concentration of 1 mL AgNPs (concentrations refer to the metal ion used in the synthesis). Assuming that all Ag^+ ions have been reduced to make AgNPs and assuming that most of the particles are spheres of 25 nm diameter, the molar concentration of AgNPs is 1.2×10^{-9} M. The cells were sampled at different time intervals such as 5, 10, 20, 30, and 60 min and visualized under HSI and confocal Raman microscope. Plasmid DNA was isolated

from untreated *E. coli* (DH5α) cells at the concentration of 100 ng μL^{-1} and incubated with AgNPs for 20 min and Raman measurements were carried out. A solution of Ag^+ ions was prepared by dissolving silver nitrate in double-distilled water at the concentration of 0.6×10^{-6} M. About 5×10^5 cells were incubated with 1 mL solution of Ag^+ ions for various incubation times and the respective samples were spotted for HSI and Raman measurements. For ITC analysis, *E. coli* was titrated against AgNPs. *E. coli* cell solution (1.62×10^{-14} M) of 40 μL was injected into 300 μL AgNPs solution (1.2×10^{-9} M) with the time spacing of 500 s between each injection.

Instrumentation Raman Spectroscopic Analysis: Confocal Raman measurements were obtained using a WiTec GmbH CRM Alpha 300 S instrument. The excitation source was 532 nm Nd:YAG laser and the maximum power output of the laser was 40 mW. The laser power was attenuated to ≈15 mW to the sampling point. Measurements were done using a 100× objective. The signal from the sample after excitation was sent to the spectrometer through a multimode fiber. The instrument has a super notch filter fixed in the path of the signal, which effectively cuts off the excitation radiation. The grating used had 600 grooves per mm, which gives a spectral resolution of 4.9 ± 1 cm^{-1}. The dispersed light intensity of the signal from the grating was measured by a Peltier-cooled charge-coupled device (CCD). The maximum area of laser exposure was 750 nm and the collection was done confocally. For most of the imaging measurements, a diffraction-limited spot size was used (the spatial resolution estimated for the 100× objective was 250 nm). The Raman images were collected with the desired area of 22 500 pixels (150 × 150) and Raman imaging was done with an integration time of 50 ms at each pixel. This imaging area corresponds to 8 × 8 μm. Single-spot spectra were taken with the integration time of 1 s. The spectra were collected in the 100–3500 cm^{-1} window. Cluster analysis of the Raman image was performed to segregate similar Raman spectra from the entire area scanned. For the Raman study, the sample solution was spotted on the cover glass and dried in ambience.

Hyperspectral Imaging Analysis: HSI measurements were performed using Cytoviva HSI system. For sample preparation, at each time point 0.5–1 μL sample was spotted on a 1-mm thick ultrasonically cleaned glass slide (SCHOTT) and it was covered with a 0.145-mm thick Nexterion Clean room cleaned glass coverslip (SCHOTT). Measurements were done using 100× oil (Cargille) immersion objective. Spectra were measured with the Specim V10E spectrometer (400–1000 nm) at the spectral resolution of ±1.5 nm. Spectral image analysis was done using the ENVI software.

Isothermal Calorimetry: ITC measurements were done using MicroCal iTC$_{200}$ system (GE Healthcare Life Sciences). Triple-distilled water was used as the reference. Sample cell contained AgNPs solution (1.2×10^{-9} M) with a maximum volume of 300 μL, while bacterial solution of 40 μL having concentration of 1.62×10^{-14} M was used as titrant with the rotation of 200 rpm. Maolarity of AgNPs and bacteria was calculated using the below formula, respectively.

$$\text{Molarity of AgNPs} = \frac{6MA_r}{\pi D^3 \rho N_A}$$

Where M = molarity of $AgNO_3$; A_r= atomic weight in g mol^{-1}; D = diameter in cm; ρ = density in g cm^{-3}; N_A = Avogadro number.

$$\text{Molarity of bacteria} = \frac{N_{E.coli} \times df}{6.023 \times 10^{23}}$$

where

$N_{E.coli}$ = Number of $E.coli$ in solution = $OD_{600} \times 10^9$; df = dilution factor

UV–Vis Spectroscopic Analysis: Ensemble-averaged UV–vis absorption spectra were recorded using a PerkinElmer Lambda 25 spectrophotometer.

Transmission Electron Microscopy Analysis: High-resolution transmission electron microscopy (HRTEM) of the sample was carried out using a JEOL 3010 instrument with an ultra high resolution (UHR) polepiece. TEM specimens were prepared by dropping one or two drops of aqueous solution to carbon-coated copper grids and drying under ambient conditions. Measurements were carried out at 200 kV.

Supporting Information

Supporting Information is available from the Wiley Online Library or from the author.

Acknowledgements

The authors thank the Department of Science and Technology (DST), Government of India for constantly supporting our research program on nanomaterials. The authors thank Dr. Nitish Mahapatra and Bhavani Shankar Sahu for providing plasmid DNA.

Received: April 24, 2013
Revised: May 23, 2013
Published online: July 1, 2013

[1] T. Pradeep, Anshup, *Thin Solid Films* **2009**, *517*, 6441.
[2] *Nanotechnology Applications for Clean Water,* (Eds: N. Savage, M. Diallo, J. Duncan, A. Street, R. Sustich), William Andrew, Norwich **2009**.
[3] M. S. Mauter, M. Elimelech, *Environ. Sci. Technol.* **2008**, *42*, 5843.
[4] D. Turkmen, V. Karakoc, L. Uzun, N. Ozturk, S. Akgol, A. Denizli, *Hacettepe J. Biol. Chem.* **2009**, *37*, 157.
[5] W. Tungittiplakorn, C. Cohen, L. W. Lion, *Environ. Sci. Technol.* **2005**, *39*, 1354.
[6] T. A. Dankovich, D. G. Gray, *Environ. Sci. Technol.* **2011**, *45*, 1992.
[7] A. D. Russell, in *Progress in Medicinal Chemistry* (Eds: G. P. Ellis, D. K. Luscombe), Elsevier Science, Amsterdam **1994**, 351–370.
[8] M. Udhaya Sankar, S. Aigal, S. M. Maliyekkal, A. Chaudhary, Anshup, A. Anil Kumar, K. Chaudhari, T. Pradeep, *Proc. Natl. Acad. Sci. USA* **2013**, *110*, 8459.
[9] M. Haruta, N. Yamada, T. Kobayashi, S. Iijima, *J. Catal.* **1989**, *115*, 301.
[10] A. S. Nair, T. Pradeep, *Curr. Sci.* **2003**, *84*, 1560.
[11] M. Conte, H. Miyamura, S. Kobayashi, V. Chechik, *J. Am. Chem. Soc.* **2009**, *131*, 7189.
[12] J. S. Kim, E. Kuk, K. M. Yu, J. H. Kim, S. J. Park, H. J. Lee, S. H. Kim, Y. K. Park, Y. H. Park, C. Y. Hwang, Y. K. Kim, Y. S. Lee, D. H. Jeong, M. H. Cho, *Nanomed. Nanotechnol. Biol. Med.* **2007**, *3*, 95.
[13] E. Hwang, J. Lee, Y. Chae, Y. Kim, B. Kim, B. Sang, M. Gu, *Small* **2008**, *4*, 746.
[14] I. Sondi, B. Salopek-Sondi, *J. Colloid Interface Sci.* **2004**, *275*, 177.
[15] W. R. Li, X. B. Xie, Q. S. Shi, H. Y. Zeng, Y. S. OU-Yang, Y. B. Chen, *Appl. Microbiol. Biotechnol.* **2010**, *85*, 1115.
[16] A. Smetana, K. Klabunde, G. Marchin, C. Sorensen, *Langmuir* **2008**, *24*, 7457.
[17] W. Yang, C. Shen, Q. Ji, H. An, J. Wang, Q. Liu, Z. Zhang, *Nanotechnology* **2009**, *20*, 085102.
[18] S. Shrivastava, T. Bera, A. Roy, G. Singh, P. Ramachandrarao, D. Dash, *Nanotechnology* **2007**, *18*, 225103.
[19] C. N. Lok, C. M. Ho, R. Chen, Q. Y. He, W. Y. Yu, H. Sun, P. K. Tam, J. F. Chiu, C. M. Chen, *J. Proteome Res.* **2006**, *5*, 916.
[20] S. K. Gogoi, P. Gopinath, A. Paul, A. Ramesh, S. S. Ghosh, A. Chattopadhyay, *Langmuir* **2006**, *22*, 9322.
[21] N. S. Wigginton, A. de Titta, F. Piccapietra, J. Dobias, V. J. Nesatyy, M. J. F. Suter, R. Bernier-Latmani, *Environ. Sci. Technol.* **2010**, *44*, 2163.

[22] R. Chen, P. Choudhary, R. N. Schurr, P. Bhattacharya, J. M. Brown, P. C. Ke, *Appl. Phys. Lett.* **2012**, *100*, 013703.
[23] S. Basu, S. Jana, S. Pande, T. Pal, *J. Colloid Interface Sci.* **2008**, *321*, 288.
[24] Z. M. Xiu, Q. B. Zhang, H. L. Puppala, V. L. Colvin, P. J. J. Alvarez, *Nano Lett.* **2012**, *12*, 4271.
[25] M. Kahraman, M. Muge Yazici, F. SahIn, O. F. Bayrak, E. TopCu, M. Culha, *Int. J. Environ. Anal. Chem.* **2007**, *87*, 763.
[26] S. Efrima, B. V. Bronk, *J. Phys. Chem. B* **1998**, *102*, 5947.
[27] R. M. Jarvis, A. Brooker, R. Goodacre, *Anal. Chem.* **2004**, *76*, 5198.
[28] A. Panacek, L. Kvitek, R. Prucek, M. Kolar, R. Vecerova, N. Pizurova, V. K. Sharma, T. Navecna, R. Zboril, *J. Phys. Chem. B* **2006**, *110*, 16248.
[29] S. Nath, S. K. Ghosh, S. Kundu, S. Praharaj, S. Panigrahi, T. Pal, *J. Nanopart. Res.* **2006**, *8*, 111.
[30] L. J. Goeller, M. R. Riley, *Appl. Spectrosc.* **2007**, *61*, 679.
[31] S. Chadha, R. Manoharan, P. Moenne-Loccoz, W. H. Nelson, W. L. Peticolas, J. F. Sperry, *Appl. Spectrosc.* **1993**, *47*, 38.
[32] Q. Wu, T. Hamilton, W. H. Nelson, S. Elliott, J. F. Sperry, M. Wu, *Anal. Chem.* **2001**, *73*, 3432.
[33] R. M. Jarvis, R. Goodacre, *FEMS Microbiol. Lett.* **2004**, *232*, 127.
[34] W. R. Premasiri, D. T. Moir, M. S. Klempner, N. Krieger, G. Jones II, L. D. Ziegler, *J. Phys. Chem. B* **2005**, *109*, 312.
[35] N. Malvadkar, P. Kao, H. Wang, D. L. Allara, M. C. Demirel, *Nanotechnology* **2008**, *2*, 555.
[36] K. A. Britton, R. A. Dalterio, W. H. Nelson, D. Britt, J. F. Sperry, *Appl. Spectrosc.* **1988**, *42*, 782.
[37] Q. Wu, W. H. Nelson, S. Elliot, J. F. Sperry, M. Feld, R. Dasari, R. Manoharan, *Anal. Chem.* **2000**, *72*, 2981.
[38] J. W. Chan, H. Winhold, M. H. Corzett, J. M. Ulloa, M. Cosman, R. Balhorn, T. Huser, *Cytometry Part A: J. Int. Soc. Anal. Cytol.* **2007**, *71*, 468.
[39] S. Singh, V. D'Britto, A. A. Prabhune, C. V. Ramana, A. Dhawan, B. L. V. Prasad, *New. J. Chem.* **2010**, *34*, 294.
[40] P. V. AshaRani, G. L. Kah Mun, M. Prakash Hande, V. Suresh, *ACS Nano* **2009**, *3*, 279.
[41] G. V. Pavan Kumar, S. Shruthi, B. Vibha, B. Ashok Reddy, T. K. Kundu, C. Narayana, *J. Phys. Chem. C* **2007**, *111*, 4388.
[42] H. Deng, V. A. Bloomfield, J. M. Benevides, G. J. Thomas Jr., *Nucl. Acids Res.* **2000**, *28*, 3379.
[43] H. Deng, V. A. Bloomfield, J. M. Benevides, G. J. Thomas Jr., *Biopolymers* **1999**, *50*, 656.
[44] D. Serban, J. M. Benevides, G. J. Thomas Jr., *Biochemistry* **2002**, *41*, 847.
[45] T. Diening, W. Ibach, in *Software Requirements and Data Analysis in Confocal Raman Microscopy* (Eds: T. Diening, O. Hollricher, J. Toporski), Springer, Berlin **2010**, 61–89.
[46] Q. L. Feng, J. Wu, G. Q. Chen, F. Z. Cui, T. N. Kim, J. O. Kim, *J. Biomed. Mater. Res.* **2000**, *52*, 662.
[47] K. B. Holt, A. J. Bard, *Biochemistry* **2005**, *44*, 13214.
[48] M. Yamanaka, K. Hara, J. Kudo, *Appl. Environ. Microbiol.* **2005**, *71*, 7589.
[49] A. Gourishankar, S. Shukla, K. N. Ganesh, M. Sastry, *J. Am. Chem. Soc.* **2004**, *126*, 13186.
[50] K. Chen, Y. Xu, S. Rana, O. R. Miranda, P. L. Dubin, V. M. Rotello, L. Sun, X. Guo, *Biomacromolecules* **2011**, *12*, 2552.
[51] J. Turkevich, P. C. Stevenson, J. Hillier, *Discuss. Faraday Soc.* **1951**, *11*, 55.